Iron-Selenide Phenomenology in Superconducting $Pr_4Fe_2As_2Te_{0.88}O_4$

C. E. Matt,[1,2] O. Ivashko,[2] M. Horio,[2] D. Sutter,[2] N. Dennler,[2] J. Choi,[2] Q. Wang,[2] M. H. Fischer,[2] S. Katrych,[3] L. Forro,[3] J. Ma,[1] B. Fu,[1] B. Lv,[1] M. v. Zimmermann,[4] T. K. Kim,[5] N. C. Plumb,[1] N. Xu,[1] M. Shi,[1] and J. Chang[2]

[1]*Swiss Light Source, Paul Scherrer Institut, CH-5232 Villigen PSI, Switzerland*
[2]*Physik-Institut, Universität Zürich, Winterthurerstrasse 190, CH-8057 Zürich, Switzerland*
[3]*Laboratory of Physics of Complex Matter, École Polytechnique Fédérale de Lausanne (EPFL), CH-1015 Lausanne, Switzerland*
[4]*Deutsches Elektronen-Synchrotron DESY, 22603 Hamburg, Germany*
[5]*Diamond Light Source, Harwell Campus, Didcot, OX11 0DE, United Kingdom*

The unified modeling of iron-based high-temperature superconductors has been complicated by different phenomenologies in the iron-pnictides and iron-chalcogenides. Here we use x-ray diffraction and angle-resolved photoemission spectroscopy to investigate the lattice and electronic properties of the $Pr_4Fe_2As_2Te_{0.88}O_4$ (T_c = 25 K) superconductor. The crystal structure undergoes a high-temperature (T_s = 250 K) orthorhombic transition with no apparent magnetic transition. Further, we find the Fermi surface to consist of zone-corner electron pockets only. In addition to superconductivity, a second electronic instability – evidenced by a spectroscopic gap below $T_g \approx 2 \times T_c$ – is found. Both, the electronic structure and the sequence of transitions, resemble what has been reported in monolayer and bulk FeSe. Our results thus provide a direct link between the iron-pnictide and iron-chalcogenide families of superconductors.

Many superconducting iron-pnictides display an intrinsic susceptibility towards nematic order which is intimately connected to an electronic spin-density-wave (SDW) instability[1–3]. Typically, superconductivity displays a competing interaction with SDW order and the interplay between all these electronic transitions provides the basis to understanding the experimentally determined phase diagrams[4,5]. This physics is remarkably robust. Similar phase diagrams and electronic structure have, for example, been obtained with $BaFe_2As_2$ as a starting point and chemical substitution on the Ba, Fe or As sites. Pursuing the goal of uncovering the origin of the superconducting and nematic instabilities triggered great efforts to reveal and understand the electronic band structure[6]. It has been found that almost all superconducting iron-pnictides display a multiband structure with hole- and electron-like Fermi-surface (FS) pockets[6]. These observations form the basis for the FS-nesting scenario between the electron and hole pockets which is employed by many theoretical models[7].

The discovery of high-temperature superconductivity in monolayer FeSe on $SrTiO_3$ (STO) substrates[8–10] has let researchers to scrutinize FeSe in both bulk and confined form. Intriguingly, FeSe displays a quite different phenomenology in comparison to the iron-pnictide compounds[11,12]. The Fermi surface of monolayer FeSe/STO, for example, consists of zone-corner electron pockets only[9,13–15]. Orthorhombicity in ambient-pressure bulk FeSe seems not connected to spin-density-wave order that develops only upon application of hydrostatic pressure[16,17]. The temperature-pressure phase diagram of FeSe suggests a completely different relation between nematicity, spin-density-wave order and superconductivity[16,18]. This remarkable contrast between FeSe and FeAs compounds poses a tremendous challenge for a global understanding of these systems. Finding an experimental link between iron-pnictides and iron-chalcogenides is therefore of great importance.

Here, we report a combined hard x-ray diffraction (XRD) and angle-resolved photoemission spectroscopy (ARPES) study of the $Pr_4Fe_2As_2Te_{0.88}O_4$ (PFATO - T_c = 25 K) superconductor[19–21]. This highly two-dimensional system is synthesized under high-pressure conditions producing small single crystals limited to $< 50 \times 50 \times 10$ μm^3 – challenging for many experimental methods. Nonetheless, we demonstrate that PFATO displays a unique set of phenomena which is in contrast to common iron-pnictide superconductors. *(i)* The crystal structure undergoes a high-temperature orthorhombic transition at T_s = 250 K. *(ii)* The Fermi surface structure consists of zone-corner electron pockets only. *(iii)* In addition to superconductivity, these electron pockets undergo an electronic transition evidenced by the opening of a gap at $T_g \approx 2 \times T_c$. In fact, these observations resemble what has been reported for iron-selenide systems. The low-temperature electronic structure of PFATO strongly resembles that of monolayer FeSe/STO. Furthermore, the large separation between orthorhombic and electronic transitions mimics the phenomenology reported in the hydrostatic pressure phase diagram of bulk FeSe. Our results thus suggest that the physics represented by FeSe can also be realized in iron-pnictides. In fact, PFATO can be regarded as a direct link between iron-pnictides and iron-chalcogenides. Our results thus pave the way for a classification of iron-based superconductors going beyond simple chemical composition. As such, our observations serve as a stepping stone for an overarching understanding of the phenomena previously associated with iron-pnictides and iron-chalcogenides.

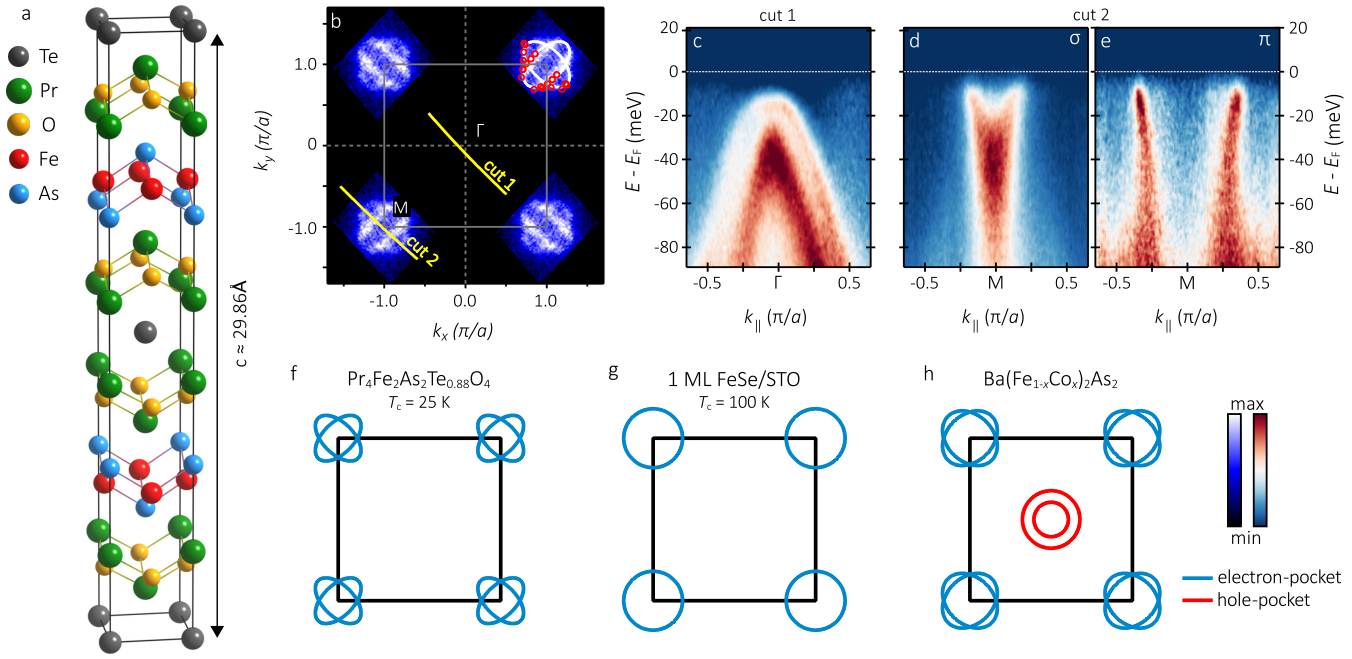

FIG. 1: **Low-energy electronic band structure of $Pr_4Fe_2As_2Te_{0.88}O_4$ (PFATO).** (a) Room temperature unit cell of $Pr_4Fe_2As_2Te_{0.88}O_4$ ($I4/mmm$ space group). (b) Symmetrized Fermi surface maps recorded on PFATO around zone corners and displayed in false color scale. The Fermi surface contours of the two electron pockets are shown schematically with solid lines in the top right zone corner. (c) Diagonal cut through the zone center reveals two hole-like bands below the Fermi level. (d - e) are diagonal cuts through the zone corner recorded with π (horizontal) and σ (vertical) light polarization that amplify either the outer or inner electron pocket. Solid red lines in (c-e) indicate the Fermi level E_F. (f-h) Schematic comparison of Fermi surface topology in PFATO, monolayer FeSe/STO and $Ba(Fe_{1-x}Co_x)_2As_2$.

Results:

Band structure: The electronic band structure measured by ARPES with diagonal cuts through the tetragonal zone center (Γ) and corner (M) is shown in Figs. 1b-e. Common to virtually all iron-based superconductors, hole (electron) bands are found around Γ (M)[22]. An unusual feature of PFATO is that the hole band maximum is located approximately 20 meV below the Fermi level. The Fermi surface thus consists of two zone-corner electron pockets only. The two electron bands can be disentangled using light polarization analysis. Inner and outer electron pockets are enhanced (turned off) for σ (π) polarization (Figs. 1d,e).

Carrier density: Our density functional theory calculation (Ref. 23, supplementary Fig. S1) of stochiometric $Pr_4Fe_2As_2TeO_4$ yields a semi-metallic structure with equal hole and electron charge carrier concentration. Just as oxygen depletion in oxides induces electron doping, reduction of Te is expected to increase the electron carrier density. Specifically, a doping of 0.12 electrons per Fe is expected in bulk $Pr_4Fe_2As_2Te_{0.88}O_4$. As will be discussed, the electron pockets are gapped at low-temperatures and hence the underlying Fermi surface contour is inferred by extrapolation. Together, the two underlying Fermi pockets amount to a filling of 0.11±0.01 electrons per Fe. This is exactly the expected bulk electron filling, suggesting that the cleaved surface is non-polar[24]. In fact, we find, using angle dependent x-ray photoemission spectroscopy (XPS), that the cleaving plane is the Te-layer (see method section and supplementary Fig. S2). PFATO therefore follows a similar cleaving behavior as found in the non-polar 122 iron-pnictide compounds. All these observations suggest that the measured band structure represents bulk properties of PFATO.

Spectral gap: A zoom-in on the low-energy spectral weight along the cut 2 (Fig. 1b) is shown in Fig. 2a,b for temperatures of 5.5 and 56 K, respectively. This weight distribution suggests much sharper quasiparticle excitations at the lowest measured temperature. This observation is supported by energy distribution curves (EDCs) at the Fermi momentum k_F indicated by the vertical dashed lines. At 5.5 K, a pronounced quasiparticle peak is observed which is not present in the 56 K spectra. Comparison of these two EDCs also evidences a leading edge gap on the low-temperature EDC. This gap, the temperature evolution, and the low-temperature momentum dependence are analyzed by symmetrized EDCs in Fig. 2d,e. To first order, 2Δ is given by the peak separation. Alternatively, the gap can be extracted by fitting the spectra using a phenomenological Green's function $G(k_F,\omega) = [(\omega + i\gamma) - \Delta/\omega]^{-1}$ where γ

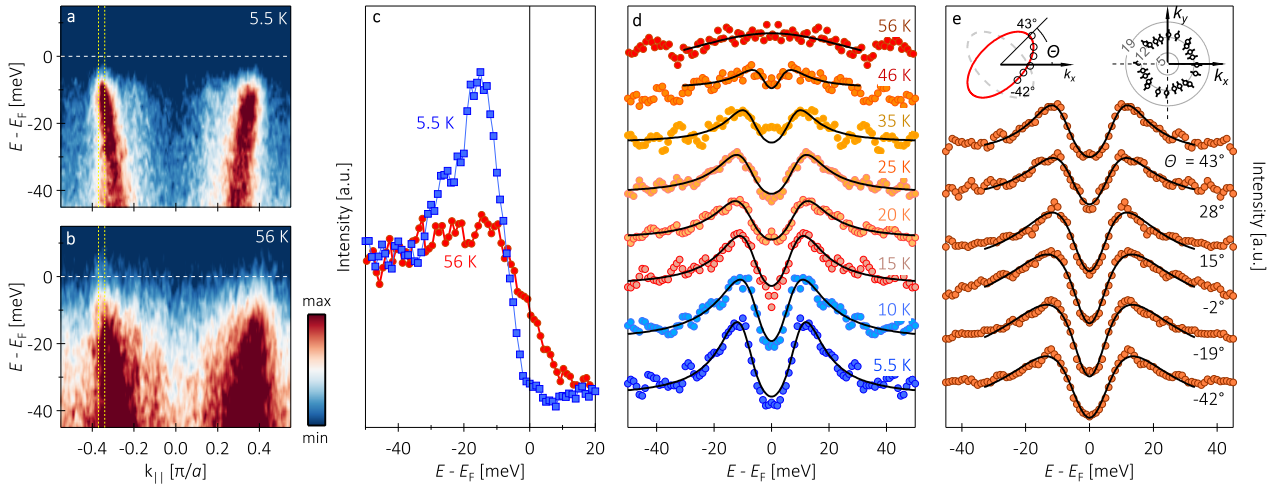

FIG. 2: **Low-temperature self-energy effects in PFATO.** (a-b) Diagonal cut through the electron pocket at M (cut 2) at 5.5 K and 56 K. c) EDCs integrated within yellow lines of b) and c) indicating closing of spectral energy gap at 56 K. As illustrated in supplementary Fig. S3, the MDC peakwidth is comparable at both temperatures, suggesting that the sample surface remains of high quality. e) Temperature dependence of the symmetrized EDC at $\theta = 43°$. The gap opening is found below $T_g \approx 50$ K. (e) Symmetrized energy distribution curves (EDCs) as a function of underlying Fermi surface angle θ, see top-left inset, obtained at 5.5 K. As visible from the spectra and as shown in the top-right-hand, this gap is essentially momentum independent. Solid lines in (d) and (e) are fits using a phenomenological Green's function to extract the gap energy scale (see text for exact explanation).

defines a scattering rate[26,27]. Irrespective of methodology, the peak position remains essentially constant at $\Delta = 14$ meV along the Fermi surface ($T < T_c$) as shown in Fig. 2e. As a function of temperature, the gap amplitude was therefore only measured along a single high symmetry direction. Intriguingly, the gap persists well into the normal state ($T > T_c$) and closes only at $T \approx 2T_c = 50$ K (Fig. 2d). It is also worth to note that the system seems to lose "coherence" simultaneously with the gap closure. Such "decoherence" behaviour has also been reported in other iron-pnictide systems[28–30].

Hierarchy of temperature scales: Orthorhombicity is revealed directly by XRD measurements of the (1,1,0) Bragg reflection as a function of temperature (Fig. 3a). Below $T_s = 250$ K, the (1,1,0) reflection splits into two satellites along the transverse direction (see inset of Fig. 3b), evidencing the existence of orthorhombicity. By analyzing the peak splitting[31], the orthorhombic (or "nematic") order parameter $\delta = (a-b)/(a+b)$ is inferred and compared to the gap temperature dependence in Fig. 3b. We notice that the appearance of the gap roughly coincides with an upturn in the resistivity and eventually the systems turns superconducting at $T_c = 25$ K (Fig. 3c). The PFATO system thus displays a hierarchy of three temperature scales. Firstly, an onset of an nematic order parameter at $T_s = 250$ K, secondly, a spectral weight gapping at $T_g = 50$ K, and finally, superconductivity below $T_c = 25$ K.

Discussion: The Fermi surface structure of iron-based superconductors typically consists of hole and electron pockets centred around the zone center and corners, respectively[6,32] (see Fig. 1h). This is, for example, the case for bulk FeSe[33], the $BaFe_2As_2$ derived 122 family[6] and the (Li, Na)FeAs derived 111 family[34,35]. Prominent exceptions are monolayer FeSe/STO ($T_c = 65 - 100$ K), $(Li_{0.84}Fe_{0.16})OHFe_{0.98}Se$ ($T_c = 41$ K), and XFe_2Se_2 (X=K, Cs) for which the Fermi surface consists of only electron pockets (Fig. 1g), while the hole band is pushed below the Fermi level[9,13,14,36,37]. In PFATO, the hole-band top is close but about 20 meV below the Fermi level. The Fermi surface therefore consists of only zone-corner electron pockets. Just as in monolayer FeSe/STO, superconductivity is emerging from these small electron pockets.

To this end, it is interesting to discuss the observed superconducting gap Δ_{sc}. Typically, iron-based superconductors – including monolayer FeSe/STO[9,14,15] – have $2\Delta_{sc}/k_BT_c \approx 5 - 6$[38]. In a few exceptional cases such as bulk FeSe $2\Delta_{sc}/k_BT_c \approx 9$ has been reported. Comparing the observed low-temperature gap amplitude Δ with the bulk transition temperature $T_c = 25$ K, yields $2\Delta/k_BT_c \approx 11$ for PFATO. This and the fact that the gap closes only at $T_g \approx 2 \times T_c$ suggests *(i)* a strong pairing interaction and presence of a pseudogap phase or *(ii)* a density-wave order emerging at T_g. Given that SDWs have been found in both iron-pnictides and iron-chalcogenides, the latter scenario appears most likely. This plausibility is based on the fact that in all known

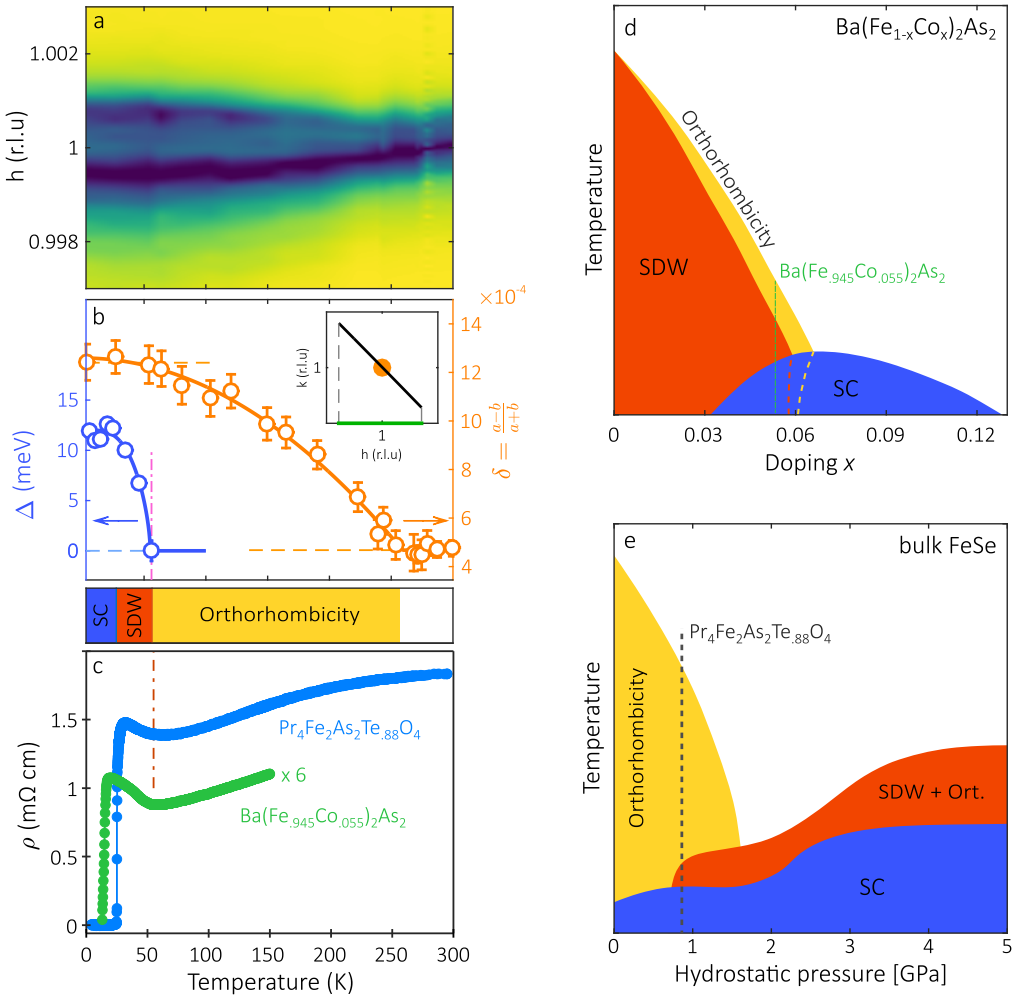

FIG. 3: **Characteristic temperature scales of $Pr_4Fe_2As_2Te_{0.88}O_4$.** (a) Diffraction intensity displayed in false color scale along the transverse direction through (1,1,0) as a function of temperature. (b) Transverse splitting of the (1,1,0) Bragg peak versus temperature along with the spectral gap amplitude Δ. (c) Resistivity curves of $Pr_4Fe_2As_2Te_{0.88}O_4$ and $Ba(Fe_{0.945}Co_{0.055})_2As_2$ adapted from Ref. 25. (d,e) Schematic phase diagrams of orthorhombicity, spin-density-wave order and superconductivity in $Ba(Fe_{1-x}Co_x)_2As_2$ and bulk FeSe. With a high-temperature onset of orthorhombicity, followed by a low-temperature electronic transformation and eventually superconductivity, PFATO resembles FeSe under pressure.

arsenide systems, orthorhombicity and SDW order is intimately connected. As shown in Fig. 3e, FeSe constitutes an example of orthorhombicity without SDW order. However, with modest hydrostatic pressure SDW order emerges in conjuction with orthorhombic lattice distortions. The observation of orthorhombic lattice distortions in PFATO therefore strongly suggest that SDW could also be present. In this context, it is worth mentioning that the resistivity (Fig. 3c) of PFATO resembles very much that of $Ba(Fe_{1-x}Co_x)_2As_2$ (see Fig. 3c), for which a SDW is well established. Finally, analysis of PFATO's magneto-resistance yields a pronounced improvement of electron mobility below T_g[21]. This is a typical effect found for density-wave transitions.

Superconducting pairing symmetry has been debated intensively in the iron-pnictides and iron-chalcogenides. The observation of high-T_c superconductivity in iron-chalcogenides emerging on electron pockets has challenged the $s^{\pm}$ paring scenario used to explain the iron-pnictide systems[7]. It has also triggered investigations to understand the role of so-called incipient bands, meaning bands that are close but not crossing the Fermi energy, in the context of superconductivity[39–41]. Spectroscopic studies of iron-selenide systems have led to contradicting results. For $A_xFe_2Se_2$ (A = K, Cs) and (Li,Fe)OHFeSe a nodeless SC gap has been reported[36,37] whereas more recent reports yield the possibility of a gap with a nodal line in FeSe[42–44]. Neutron spectroscopy reports of spin resonances are also indicative of a sign-changing order parameter[45,46]. The exact pairing symmetry and the exact role of the incipient hole band are, however, not clarified. In PFATO the situation is similar. The superconducting

gap emerging on zone-corner electron pockets provides no evidence of gap nodes. However, the fact that spectral weight gapping extends far into the normal state suggests that the system has two gapping mechanisms. This certainly complicates extraction of the superconducting gap symmetry and the role of the incipient hole band.

In summary, our results on $Pr_4Fe_2As_2Te_{0.88}O_4$ demonstrate electronic structure and a hierarchy of temperature scales resembling what has been reported on iron-chalcogenide superconductors. The Fermi surface consists of zone-corner pockets only, challenging all electron-hole pocket nesting scenarios. Furthermore, a high-temperature onset of a nematic order parameter seems uncorrelated with the low-temperature Fermi surface instabilities. As shown schematically in Fig. 3e, this sequence of transitions mimics observations found in the bulk FeSe pressure phase diagram[18] and it is inconsistent with the established phenomenology of common iron-pnictide superconductors (Fig. 3d). $Pr_4Fe_2As_2Te_{0.88}O_4$ therefore constitutes a link between iron-pnictides and iron-chalcogenides and hence, provides the perspective of having a single overarching description of iron-based superconductors.

Acknowledgements: We are grateful to Jörg Schmalian for discussions. Acknowledgements goes to Diamond Light Source for time on beamline I05 under proposal SI16104 and thank all the beamline staff for technical support. C.E.M acknowledges support from the Swiss National Science Foundation under grant No. 200021-137783 and P2EZP2_175155. O.I., M.H., J.C., D.S, and J.C. acknowledge support from the Swiss National Science Foundation under grant No. BSSGIO_155873, PP00P2_150573 and through the Sinergia Network Mott Physics Beyond the Heisenberg Model.

Authors contributions: SK and LF grew single crystals of $Pr_4Fe_2As_2Te_{0.88}O_4$. CEM, MH, DS, TKK, NX, JMand JC carried out the ARPES experiments. ND, JC, OI, MvZ and JC conducted the x-ray diffraction experiments. CEM prepared the samples for both the ARPES and XRD experiments. MHF, QW, and JC supervised the project. MS and NCP initiated the project. All authors contributed to the manuscript.

Methods

High-quality single crystals of $Pr_4Fe_2As_2Te_{0.88}O_4$ were synthesized by high-pressure flux-growth. Previous X-ray diffraction measurements have shown that, at room temperature (RT), PFATO crystallizes in a tetragonal *I4/mmm* crystal structure (see Fig. 1a) with lattice parameters $a = 4.02$ and $c = 29.86$ Å[19].The largest crystals – $50 \times 50 \times 10$ μm^3 – were selected for ARPES and high-resolution x-ray diffraction (XRD) experiments. Due to the small sample size, the diffraction experiment demands a high-flux synchrotron beamline. Our XRD experiment was carried out on the P07 beamline at PETRA III (DESY-Hamburg). A $Pr_4Fe_2As_2Te_{0.88}O_4$ crystal was mounted on the apex of a cactus needle to ensure sufficiently low background scattering. The sample was cooled inside a 10 T cryomagnet and oriented to access the $(h, k, 0)$ scattering plane. Due to the small sample mass, the strongest measured Bragg reflection gave only 10 counts/ms using high-resolution mono-chromator settings. ARPES experiments were carried out at both the SIS and I05 beamlines – Swiss Light Source, Switzerland and Diamond, UK respectively. Pristine surfaces were obtained through a top post cleaving method. Angle dependent x-ray photoelectron spectroscopy (XPS) measurements prove that the cleaving plane is the charge neutral Te layer (see supplementary Fig. S2). Thermal and electrical grounding were realized through a combination of silver epoxy and graphite paste. Commercial Scienta analysers were used at both beam lines. The Fermi level was estimated from a reference spectra of gold or copper in electrical contact with the PFATO sample.

Data availability

The data sets that support the findings in this study are available from the corresponding authors upon reasonable request.

Competing interest

The Authors declare no Competing Financial or Non-Financial Interests.

Additional information

Correspondence to: J. Chang (johan.chang@physik.uzh.ch) and C.E. Matt (cmatt@g.harvard.edu).

[1] Chu, J.-H. *et al.* In-plane resistivity anisotropy in an underdoped iron arsenide superconductor **329**, 824–826 (2010).

[2] Fernandes, R. M., Chubukov, A. V. & Schmalian, J. What drives nematic order in iron-based superconductors? *Nature Physics* **10**, 97–104 (2014).

[3] Stewart, G. R. Superconductivity in iron compounds. *Rev. Mod. Phys.* **83**, 1589–1652 (2011).

[4] Paglione, J. & Greene, R. L. High-temperature superconductivity in iron-based materials. *Nature Physics* **6**, 645 (2010).

[5] Basov, D. N. & Chubukov, A. V. Manifesto for a higher Tc. *Nature Physics* **7**, 272 (2011).

[6] Richard, P. *et al.* Fe-based superconductors: an angle-resolved photoemission spectroscopy perspective. *Reports on Progress in Physics* **74**, 124512 (2011).

[7] Chubukov, A. Pairing Mechanism in Fe-Based Superconductors. *Annual Review of Condensed Matter Physics*

3, 57–92 (2012). https://doi.org/10.1146/annurev-conmatphys-020911-125055.

[8] Qing-Yan, W. *et al.* Interface-Induced High-Temperature Superconductivity in Single Unit-Cell FeSe Films on $SrTiO_3$. *Chinese Physics Letters* **29**, 037402 (2012).

[9] He, S. *et al.* Phase diagram and electronic indication of high-temperature superconductivity at 65 K in single-layer FeSe films. *Nature Materials* **12**, 605 (2013).

[10] Ge, J.-F. *et al.* Superconductivity above 100 K in single-layer FeSe films on doped $SrTiO_3$. *Nature Materials* **14**, 285 (2015).

[11] Böhmer, A. E. & Kreisel, A. Nematicity, magnetism and superconductivity in FeSe. *Journal of Physics: Condensed Matter* **30**, 023001 (2018).

[12] Dagotto, E. Colloquium: The unexpected properties of alkali metal iron selenide superconductors. *Rev. Mod. Phys.* **85**, 849–867 (2013).

[13] Liu, D. *et al.* Electronic origin of high-temperature superconductivity in single-layer FeSe superconductor. *Nature Communications* **3**, 931 (2012).

[14] Tan, S. *et al.* Interface-induced superconductivity and strain-dependent spin density waves in $FeSe/SrTiO_3$ thin films. *Nature Materials* **12**, 634 (2013).

[15] Lee, J. J. *et al.* Interfacial mode coupling as the origin of the enhancement of T_c in FeSe films on $SrTiO_3$. *Nature* **515**, 245 (2014).

[16] Sun, J. P. *et al.* Dome-shaped magnetic order competing with high-temperature superconductivity at high pressures in FeSe. *Nature Communications* **7**, 12146 (2016).

[17] Khasanov, R. *et al.* Pressure-induced magnetic order in FeSe: A muon spin rotation study. *Physical Review B* **95**, 180504 (2017).

[18] Kothapalli, K. *et al.* Strong cooperative coupling of pressure-induced magnetic order and nematicity in FeSe **7**, 12728 (2016).

[19] Katrych, S. *et al.* $L_4Fe_2As_2Te_{1-x}O_{4-y}F_y$($L$ = Pr, Sm, Gd) : A layered oxypnictide superconductor with T_c up to 45 K. *Phys. Rev. B* **89**, 024518 (2014).

[20] Katrych, S. *et al.* $Pr_4Fe_2As_2Te_{1-x}O_4$: A layered FeAs-based superconductor. *Phys. Rev. B* **87**, 180508 (2013).

[21] Pisoni, A. *et al.* Magnetotransport studies of superconducting $Pr_4Fe_2As_2Te_{1-x}O_4$. *Phys. Rev. B* **93**, 094519 (2016).

[22] Sunagawa, M. *et al.* Characteristic two-dimensional Fermi surface topology of high-Tc iron-based superconductors. *Scientific Reports* **4**, 4381 (2014).

[23] Bucci, F. *et al.* 42214 layered Fe-based superconductors: An ab initio study of their structural, magnetic, and electronic properties. *Phys. Rev. B* **93**, 024518 (2016).

[24] Nakagawa, N., Hwang, H. Y. & Muller, D. A. Why some interfaces cannot be sharp. *Nature Materials* **5**, 204–209 (2006).

[25] Rullier-Albenque, F. *et al.* Hall Effect and Resistivity Study of the Magnetic Transition, Carrier Content, and Fermi-Liquid Behavior in $Ba(Fe_{1-x}Co_x)_2As_2$. *Physical Review Letters* **103**, 057001 (2009).

[26] Norman, M. R. *et al.* Phenomenology of the low-energy spectral function in high-T_c superconductors. *Phys. Rev. B* **57**, R11093–R11096 (1998).

[27] Matt, C. E. *et al.* Electron scattering, charge order, and pseudogap physics in $La_{1.6-x}Nd_{0.4}Sr_xCuO_4$: An angle-resolved photoemission spectroscopy study. *Phys. Rev. B* **92**, 134524 (2015).

[28] Zhang, Y. *et al.* Nodal superconducting-gap structure in ferropnictide superconductor $BaFe_2(As_{0.7}P_{0.3})_2$. *Nature Physics* **8**, 371–375 (2012).

[29] Terashima, K. *et al.* Fermi surface nesting induced strong pairing in iron-based superconductors. *Proceedings of the National Academy of Sciences* **106**, 7330–7333 (2009).

[30] Huang, J. *et al.* Emergence of Superconductivity from Fully Incoherent Normal State in an Iron-Based Superconductor $(Ba_{0.6}K_{0.4})Fe_2As_2$. *Science Bulletin* **64**, 11–19 (2019).

[31] McIntyre, G. J., Renault, A. & Collin, G. Domain and crystal structure of superconducting $Ba_2YCu_3O_{8-\delta}$ at 40 and 100 K by single-crystal neutron diffraction. *Phys. Rev. B* **37**, 5148–5157 (1988).

[32] Ye, Z. R. *et al.* Extraordinary Doping Effects on Quasiparticle Scattering and Bandwidth in Iron-Based Superconductors. *Physical Review X* **4**, 031041 (2014).

[33] Liu, X. *et al.* Electronic structure and superconductivity of fese-related superconductors. *Journal of Physics: Condensed Matter* **27**, 183201 (2015).

[34] Borisenko, S. V. *et al.* Superconductivity without Nesting in LiFeAs. *Physical Review Letters* **105**, 067002 (2010).

[35] He, C. *et al.* Electronic-Structure-Driven Magnetic and Structure Transitions in Superconducting NaFeAs Single Crystals Measured by Angle-Resolved Photoemission Spectroscopy. *Physical Review Letters* **105**, 117002 (2010).

[36] Zhao, L. *et al.* Common electronic origin of superconductivity in (Li,Fe)OHFeSe bulk superconductor and single-layer $FeSe/SrTiO_3$ films. *Nature Communications* **7**, 10608 (2016).

[37] Zhang, Y. *et al.* Nodeless superconducting gap in $AxFe_2Se_2$ (A=K,Cs) revealed by angle-resolved photoemission spectroscopy. *Nature Materials* **10**, 273 (2011).

[38] Inosov, D. S. *et al.* Crossover from weak to strong pairing in unconventional superconductors. *Phys. Rev. B* **83**, 214520 (2011).

[39] Chen, X. *et al.* Electron pairing in the presence of incipient bands in iron-based superconductors. *Phys. Rev. B* **92**, 224514 (2015).

[40] Maier, T. A. *et al.* Effective pairing interaction in a system with an incipient band. *Phys. Rev. B* **99**, 140504 (2019).

[41] Miao, H. *et al.* Observation of strong electron pairing on bands without Fermi surfaces in $LiFe_{1x}Co_xAs$. *Nature Communications* **6**, 6056 (2015).

[42] Sprau, P. O. *et al.* Discovery of orbital-selective Cooper pairing in FeSe. *Science* **357**, 75–80 (2017).

[43] Rhodes, L. C. *et al.* Scaling of the superconducting gap with orbital character in FeSe. *Phys. Rev. B* **98**, 180503 (2018).

[44] Liu, D. *et al.* Orbital origin of extremely anisotropic superconducting gap in nematic phase of FeSe superconductor. *Phys. Rev. X* **8**, 031033 (2018).

[45] Wang, Q. *et al.* Transition from sign-reversed to sign-preserved cooper-pairing symmetry in sulfur-doped iron selenide superconductors. *Phys. Rev. Lett.* **116**, 197004 (2016).

[46] Pan, B. *et al.* Structure of spin excitations in heavily electron-doped $Li_{0.8}Fe_{0.2}$ODFeSe superconductors. *Nature Communications* **8**, 123 (2017).